J Appl Electrochem (2009) 39:2421–2431
DOI 10.1007/s10800-009-9930-2

ORIGINAL PAPER

Carbon nano-tube supported Pt–Pd as methanol-resistant oxygen reduction electrocatalyts for enhancing catalytic activity in DMFCs

Ahmad Nozad Golikand · Elaheh Lohrasbi · Mohammad Ghannadi Maragheh · Mehdi Asgari

Received: 15 January 2009 / Accepted: 7 May 2009 / Published online: 28 May 2009
© Springer Science+Business Media B.V. 2009

Abstract This work tries to study the problem of methanol crossover through the polymer electrolyte in direct methanol fuel cells (DMFCs) by developing new cathode electrocatalysts. For this purpose, a series of gas diffusion electrodes (GDEs) were prepared by using single-walled carbon nanotubes (SWCNTs) supported Pt–Pd (Pt–Pd/SWCNT) with different Pd contents at the fixed metal loading of 50 wt%, as bimetallic electrocatalysts, in the catalyst layer. Pt–Pd/SWCNT was prepared by depositing the Pt and Pd nanoparticles on a SWCNTs support. The elemental compositions of bimetallic catalysts were characterized by inductively coupled plasma atomic emission spectroscopy (ICP-AES) system. The performances of the GDEs in the methanol oxidation reaction (MOR) and in the oxygen reduction reaction with/without the effect of methanol oxidation reaction were investigated by means of electrochemical techniques: cyclic voltammetry (CV), linear sweep voltammetry (LSV), and electrochemical impedance spectroscopy (EIS). The results indicated that GDEs with Pt–Pd/SWCNT possess excellent electrocatalytic properties for oxygen reduction reaction in the presence of methanol, which can originate from the presence of Pd atoms and from the composition effect.

Keywords Direct methanol fuel cell · Oxygen reduction · Gas diffusion electrode · Methanol-resistant · Bimetallic electrocatalyst

A. N. Golikand (✉) · M. G. Maragheh · M. Asgari
Jaber Ibne Hayan Research Labs, NSTRI, Tehran, Iran
e-mail: anozad@aeoi.org.ir

A. N. Golikand · E. Lohrasbi
Corrosion Lab, Material School, NSTRI, Tehran, Iran

1 Introduction

Direct methanol fuel cells (DMFCs) provide significant advantages, such as high energy density, low pollution, rapid start-up, and compactness over rechargeable batteries, and other types of fuel cells for portable applications [1].

A simple schematic of the DMFC is shown in Fig. 1. The fuel (methanol and water) passes through the anode, and the oxidant (O_2 in air) flows through the cathode. The two electrodes are separated by a proton exchange membrane such as Nafion. Platinum-based electrodes demonstrate the highest catalytic activity and the cleanest combustion products. Since engines operate at high temperatures, this whole system will be in an "oven-like" setting. The design and construction of high-performance DMFCs has already been undergoing optimization [2].

The DMFC performance is still hindered by several factors including the high costs of the Pt-based electrocatalysts, the poor kinetics of both anode [3], and cathode reactions [4] and the crossover of methanol from the anode to the cathode through the proton exchange membranes [5, 6]. The methanol crossover from the anode to the cathode poisons the Pt catalyst and causes the mixed potentials, which decrease the fuel cell performance [7, 8]. The polarization losses are caused mainly because methanol is oxidized heterogeneously in the presence of oxygen [9]. Methanol electro-oxidation at platinum is a self-poisoning reaction, as strongly adsorbed CO is formed by dehydrogenation of methanol, which blocks the surface for further methanol adsorption and leads to very low DMFC power densities [10].

This poisoning effect ultimately results in instability as well as in a reduction in cell performance. In order to address the crossover problem, one strategy is the use of

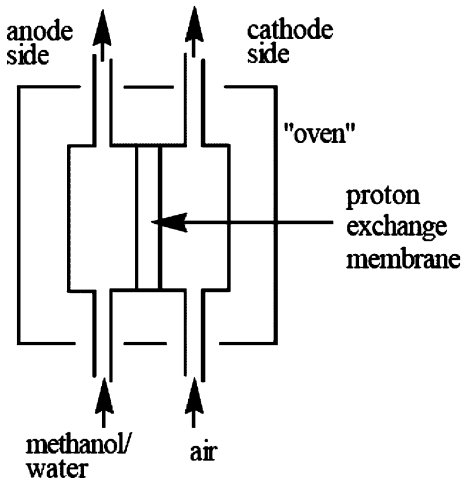

Fig. 1 A simple schematic of a DMFC

electrolytes with lower methanol permeability. The other strategy is the development of novel oxygen reduction reaction (ORR) electrocatalysts with both higher methanol tolerance and higher activity for the ORR than Pt. Higher methanol tolerance has been reported in the literature for non-noble metal electrocatalysts based on ruthenium chalcogenide catalysts [11, 12] and macrocycles of transition metals [13, 14]. These electrocatalysts have shown nearly the same activity for the ORR in the absence as well as in the presence of methanol. Developing a sufficiently selective and active electrocatalyst for the DMFC cathode remains one of the key tasks for further progress of this technology. Catalysts with lower methanol oxidation reaction (MOR) activity than Pt, which decrease the mixed potential [5, 15] and, on the other hand, catalysts with higher MOR activity, which decrease CO poisoning have been investigated [16, 17].

Catalysts with lower MOR activity are of two kinds: catalysts with lower MOR by reduced CH_3OH dissociative adsorption [18–21], and catalysts with lower MOR activity by reduced CO oxidation [22–24]. The main way to reduce methanol adsorption is the so-called "ensemble effect." It happens when the active component is diluted by inert metals by forming bimetallic catalysts that causes changes in the distribution of active sites and open different reaction pathways [25]. The dissociative chemisorption of methanol requires the existence of several adjacent Pt ensembles [26, 27] and the presence of the atoms of a second metal around the active sites of Pt could block methanol adsorption on the Pt sites due to the dilution effect.

For example, carbon supported Pt–Ni electrocatalysts in the Pt:Ni atomic ratios of 90:10 and 70:30 were prepared by Antolini et al. [28] by the reduction at room temperature of Pt and Ni salts with sodium borohydride and tested in direct methanol fuel cells both as anode and cathode materials. The ORR activity of Pt–Ni/C electrocatalyst in the Pt:Ni atomic ratio of 70:30 was investigated in sulfuric acid both in the absence and presence of methanol [29]. In methanol-free sulfuric acid, the Pt–Ni/C alloy catalyst showed a lower specific activity toward the oxygen reduction compared to pure platinum. In O_2-free H_2SO_4, the onset potential for methanol oxidation at Pt–Ni/C shifted to more positive potential, indicative of a lower activity for the methanol oxidation than platinum. The higher ORR activity in the methanol-containing electrolyte of Pt–Ni/C electrocatalyst was ascribed to the low activity of the binary electrocatalyst for methanol oxidation, arising from a composition effect.

Stassi et al. [30] prepared 60 wt% Pt–Fe/C and Pt–Cu/C catalysts. Polarization curves of ORR for Pt, Pt–Cu, and Pt–Fe in oxygen saturated H_2SO_4 solution showed that onset potential for the ORR on Pt–Fe catalyst shifted toward the positive potential, which indicates better catalytic characteristics of this catalyst for ORR compared to the previous ones. The onset potential for the ORR on the Pt–Fe catalyst is less negatively shifted in the presence of methanol than on the Pt catalyst.

An alternate approach to prevent the loss of unit cell performance by methanol crossover and to assure the long-term stability of cell performance is to prevent the poisoning of Pt by removing the CO adsorbed in the Pt. According to the bifunctional and electronic effects, well-known in designing of alloy catalysts for methanol oxidation at anode in DMFC [31–33], Pt-based alloy catalysts can be prepared for oxygen reduction so that the Pt is not poisoned. During alloy formation, the presence of a second metal can remove CO poisoning of Pt catalyst and, at the same time, it does not affect the catalytic activity for oxygen reduction to any extent.

Park et al. [34] synthesized unsupported Pt–Rh alloy nanoparticles in the Pt:Rh atomic ratios 3:1, 2:1, and 1:1 by the reduction of Pt and Rh precursors at room temperature with $NaBH_4$, and investigated their ORR activity and methanol tolerance by LSV measurements and tests in DMFCs. Linear sweep voltammetry of Pt, Pt–Ru, and Pt–Rh for methanol oxidation in 0.5 M H_2SO_4 + 2 M CH_3OH indicated that Pt–Ru nanoparticles possess the optimal catalytic activity for methanol oxidation. Even if further studies are needed to clarify the mechanism of the enhanced activity of Pt–Rh alloy, the authors concluded that the alloy may contribute to enhanced CO oxidation. Our previous study [16] showed that the activity of electrodeposited Pt–Sn bimetallic particles for MOR was higher than that of the acknowledged Pt–Ru particles.

As reported by Mukerjee et al. [35], the formation of a Pt–M alloy gives rise to two counteracting effects: a decrease in MOR activity by the dilution effect or an increase in MOR activity due to the presence of M that

reduces the Pt–CO bond strength substantially and subsequently enhances the oxidation of CO.

Greeley et al. showed that the closer the position of ε_d toward the Fermi level, the stronger the interactions with the adsorbates [36]. Their calculations also showed a linear correlation between the O binding energies and the d-band position of the Pd atom on M surfaces (Fig. 2A). Pd/Ru (0001), Pd/Ir (111), and Pd/Rh (111) lie at the upper left end of the plot with a low ε_d (i.e., a weak interaction between O and the Pd monolayer), whereas Pd/Au (111) lies at the lower right end with a high ε_d, with a correspondingly strong interaction. Following Sabatier's principle, a good ORR electrocatalyst may exhibit a moderate interaction with the adsorbates. Thus, Pd/Ru (0001), Pd/Ir (111), and Pd/Rh (111) are not expected to be very active due to their slow kinetics in breaking O–O bonds, whereas Pd/Au (111) with ε_d close to the Fermi level bonds strongly with O; thereby hinders the subsequent reaction steps and slows the kinetics of oxygen reduction. However, Pd/Pt (111) with ε_d lying in the middle and, therefore, forming a moderate bond with the adsorbents may be a good catalyst for the ORR. When the half-wave potentials obtained experimentally are plotted against the calculated d-band center, a volcano-type variation in the measured ORR activity of Pd/M is observed with the increasing d-band of Pd (Fig. 2B). In agreement with the theoretical predications, Pd/Pt (111) that has a moderate ε_d value and, therefore, a moderate activity, is the best catalyst for ORR. Accordingly, it is a very active electrocatalyst for oxygen reduction in acidic solutions.

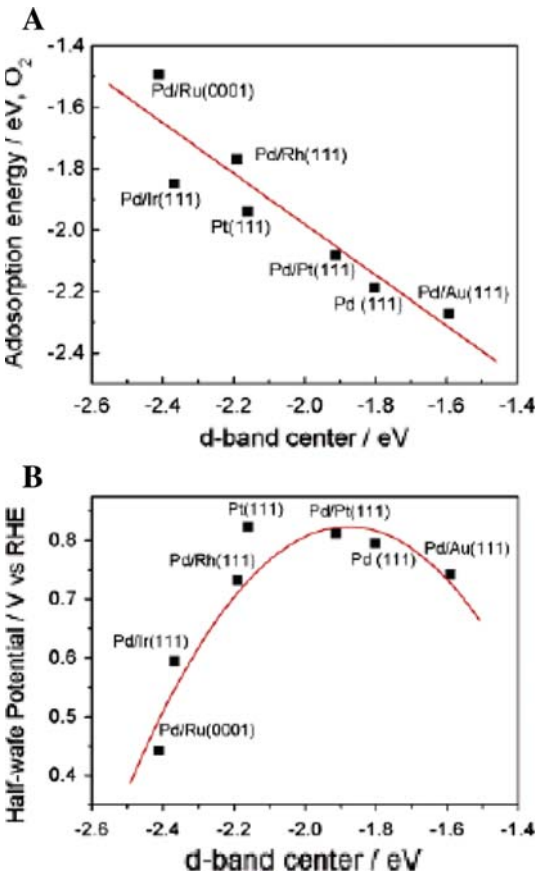

Fig. 2 The calculated O_2 adsorption energies on Pd monolayers on various substrates (**A**) and half-wave potentials for the ORR on Pd monolayers on different substrates in a 0.1 M $HClO_4$ solution (**B**) both as a function of the calculated Pd d-band center (relative to the Fermi level). The Pt (111) data are included for comparison [38]

The miniaturization of fuel cells requires sub-micrometer-sized conductive support electrodes. Therefore, single- and multi-walled carbon nanotubes have been recently used to support the catalysts with a high surface area for developing electrode materials for DMFC, in addition to the often-used electrically conducting carbon film. The structure of single-walled CNTs (SWNTs) is nearly perfect, even after functionalization, while other types of CNTs contain a significant concentration of structural defects in their walls [37].

In this research, concentration on the preparation of gas diffusion electrodes using carbon nano-tube supported Pt–Pd bimetallic catalysts. The effects of the composition and structure of the catalysts on ORR activity were also evaluated in the absence and presence of methanol.

Three layer gas diffusion electrodes (GDEs) were chosen for the present investigation. Figure 3 shows a schematic illustration of the three layer gas diffusion electrodes. The electrodes are based on a porous carbon layer, typically carbon paper or carbon cloth. In the present study, we used carbon paper as substrate. The gas diffusion layer (GDL) is the electrical conductor that transports the electrons to and from the catalyst layer.

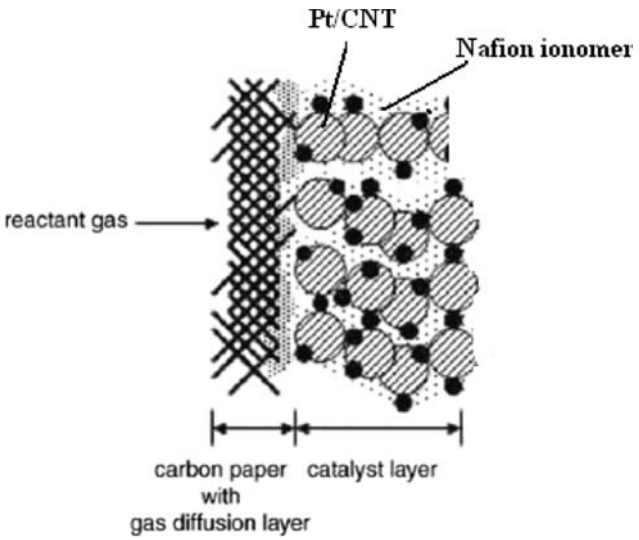

Fig. 3 A simple schematic of a GDE

The gas diffusion layer also assists in water management by allowing an appropriate amount of water to reach and to remain at the membrane for hydration. Furthermore, gas diffusion layers are typically wet-proofed with Teflon (PTFE) coating to ensure that the pores of the gas diffusion layer do not become congested with liquid water.

The electrocatalyst and ionomer were mixed in a solvent to form the catalyst layer. Currently, Nafion is often the ionomer of choice for the catalyst layer both as a proton conductor and as a binder in the electrodes.

In the three-electrode tests, various electrochemical techniques such as cyclic voltammetry, linear sweep voltammetry, and AC impedance spectroscopy are used. Bimetallic catalysts were characterized by X-ray diffraction and ICP.

2 Experimental

2.1 Surface modification of SWCNTS

Previous work in our lab has shown that treatment of carbon with concentrated nitric acid increases its hydrophilicity by forming surface carboxylic acid functionality [38]. Therefore, the surfaces of commercial SWCNTs (Aldrich, OD: 1–2 nm, length 20–40 μm, purity 20–30%) were functionalized with carboxyl functional groups. For this purpose, the commercial SWCNT and concentrated nitric acid were refluxed at 140 °C for 7 h. It was then washed well with deionized water and dried to produce a modified catalyst.

2.2 Electrocatalyst preparation

In order to support Pt nanoparticles on the SWCNTs, we adopted the well-known impregnation method followed by liquid-phase borohydride. A mixture of modified SWCNTs and H_2PtCl_6 (Aldrich) and (to prepare bimetallic catalysts), appropriate amounts of 0.1 M solution of transition metal salts ($PdCl_2$) (Merck) were suspended by sonication in 40 mL of deionized water. Subsequently, these metals were reduced and supported on the SWCNTs simultaneously by $NaBH_4$ (Kanto Chemical) as the reducing agent. Then they were washed with deionized water several times. The filtrate was collected to determine the exact load of Pt by measuring the Pt residue. After drying, the SWCNT supported Pt–Pd nanoparticles were obtained. In order to study the effect of composition on the performance of electrodes with Pt–Pd catalysts, which exhibited better performance than others, we prepared the Pt–Pd bimetallics with different compositions (1:1, 3:1, and 9:1 atomic ratios).

The analysis of atomic composition of the catalysts was performed using an IRIS advantage inductively coupled plasma atomic emission spectroscopy (ICP-AES) system (Varian Austria).

2.3 Fabrication of gas diffusion electrode and electrochemical measurements

Porous GDEs were constructed according to a previously described procedure [39].

In order to prepare the PTFE-bonded porous GDL, a commercially available carbon Vulcan (XC-72R from ElectroChem. Inc.) 70 and 30% PTFE (from ElectroChem. Inc.) emulsions were used and painted onto carbon paper TGP-H-0120 (Toray).

The resulting composite structure was dried in air at 80–90 °C for 1 h, followed by thermal treatment at 250 °C for 30 min to remove the dispersion agent contained in the PTFE, and finally sintered in air at 340 °C for 15 min. The PTFE is effective as a binder and imparts hydrophobicity to the gas diffusion regime of the electrodes.

In order to prepare the catalyst layer, a mixture comprising of a homogeneous suspension of Nafion, Pt/CNT 50%, or Pt–Pd/CNT 50% catalyst with different compositions (see Table 1) and Isopropyl alcohol as solvent was homogenized using a sonicator (Misonix Model S-3000) for 20 min. The ink was painted on the GDL. The resulting composite structure was dried in air at 25 °C for 1 h, and finally sintered in air at 140 °C (above the glass transition temperature of Nafion [40]) for 45 min.

The Nafion and Pt loadings were 1 and 0.5 mg cm^{-2} in the GDE, respectively. The reduction of oxygen was investigated using the porous GDE (geometric exposed area of 1.3 cm^2) in 2 M H_2SO_4 solution. Linear sweep voltammetry (LSV) measurements were carried out at 298 K in a conventional three-electrode cell with O_2 flow rate of 50 mL min^{-1}. Cyclic voltammetry (CV) experiments were done at 298 K in a conventional three-electrode cell. The GDEs were mounted in a Teflon holder containing a high pyrolytic graphite disk as a current collector (which had an arrangement for oxygen feed from the back of the electrode). A large-area platinum flat electrode was used as the

Table 1 Number of GDEs and bimetallic catalysts' compositions extracted from ICP

Number of GDEs	Catalyst that used in catalyst layer	Pt:Pd atomic ratio (ICP)	Pd content in catalysts (%)
GDE1	Pt	–	0
GDE2	Pt–Pd	9:1	10
GDE3	Pt–Pd	3:1	25
GDE4	Pt–Pd	1:1	50

counter electrode. An Ag/AgCl reference electrode was placed close to the working electrode surface. The electrochemical cell was connected to a potentiostat/galvanostat (Radiometer Model DEA332) digital electrochemical analyzer equipped with an IMT 102 electrochemical interface for CV and LSV, and also to a computer controlled 30(2) Autolab electrochemical system (EcoChemie, Utrecht, Netherlands), driven with GPES and FRA softwares (EcoChemie) for electrochemical impedance spectroscopy (EIS). In the present study, AC potential amplitude of 5 mV in a frequency range 10 mHz–2.6 kHz was applied.

3 Results and discussion

3.1 Oxygen reduction reaction on GDEs

Figure 4 provides an ORR comparison on the GDEs under similar experimental conditions. Clearly, among all the GDEs, GDE1 displayed the lowest ORR activity. GDE2 showed the highest catalytic activity for ORR among the other GDEs. The onset potential for oxygen reduction on this GDE shifted to more positive potentials. The enhanced catalytic activity is attributed to a good combination of some factors including the change in Pt–Pt interatomic distance, the number of Pt nearest neighbors [41, 42], and also to Sabatier's principle. Following to Sabatier's principle [37], a good ORR electrocatalyst may exhibits a moderate interaction with the adsorbates. Pt–Pd that has a moderate ε_d value and, therefore, a moderate activity is the best catalyst for ORR.

This result also shows that the higher Pd content in GDE3 and GDE4 decreases the Pt d-bond vacancy [43], blocks Pt active sites, decreases the steady-state concentration of the absorbed oxygen on the cathode, and hinders oxygen reduction. Therefore, GDE2 has an optimum content of Pd atoms (10%) by providing the highest catalytic activity for ORR.

3.2 Methanol oxidation on GDEs

Moreover, to understand the origin of the high methanol tolerance of Pt–Pd bimetallic catalysts during the ORR, methanol oxidation in argon saturated 2 M H_2SO_4 + 2 M CH_3OH solution was studied under similar experimental conditions (data are shown in Fig. 5). The methanol-containing electrolyte was previously purged with argon in order to avoid oxygen contamination. It was found that the current densities of the MOR on GDE1 are much higher than those on the other GDEs and that the onset potential for methanol oxidation on GDE4, GDE3, and GDE2 (GDEs with Pt–Pd catalysts) shifted to more positive potentials as compared to GDE1, this indicates that the GDEs with bimetallic catalysts for methanol oxidation were less active than GDE1 with pure Pt catalyst, which could be induced by the composition effect and by the presence of Pd atoms in the catalysts (Ensemble effect, which happens when the active component is diluted by catalytically inert metals by forming bimetallic catalysts that causes changes in the distribution of active sites and opens different reaction pathways [25].). The dissociative

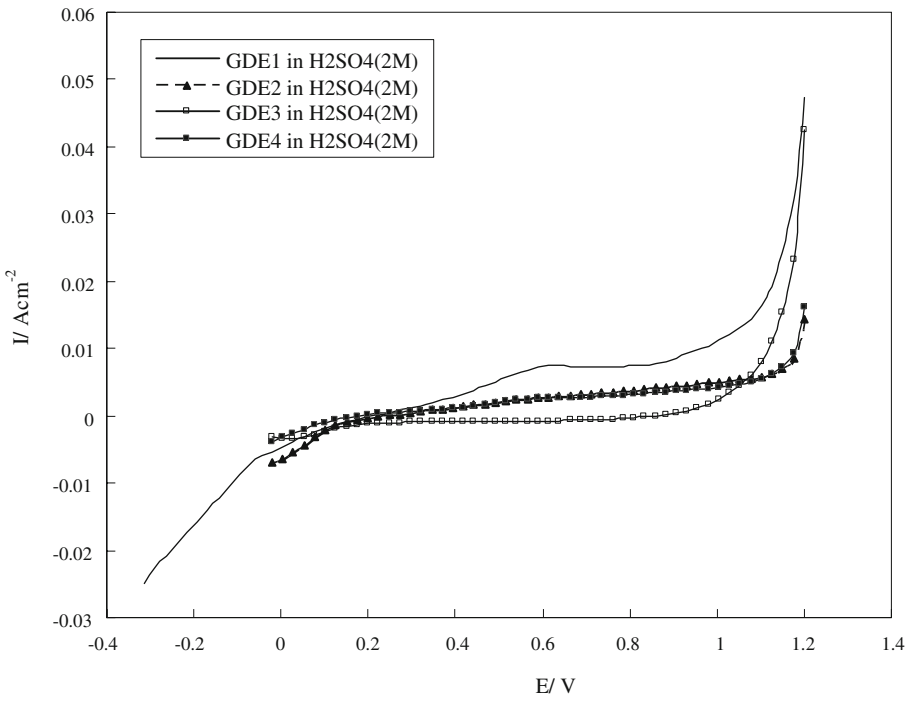

Fig. 4 Linear sweep voltammograms of ORR on GDEs in oxygen saturated 2 M H_2SO_4 and the scan rate of 5 mV s^{-1}

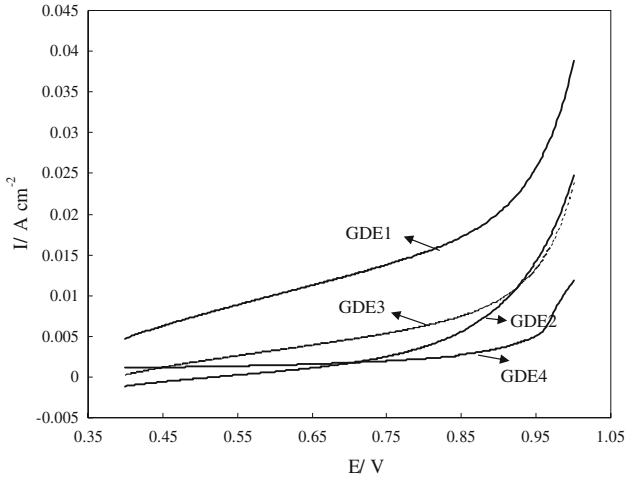

Fig. 5 Linear sweep voltammograms of methanol oxidation on GDEs in argon saturated 2 M H_2SO_4 + 2 M CH_3OH and the scan rate of 5 mV s^{-1}

chemisorption of methanol requires the existence of several adjacent Pt ensembles [26, 27] and the presence of the atoms of a second metal around the active sites of Pt could block methanol adsorption on the Pt sites due to the dilution effect. It is known that Pd has no electrocatalytic activity for alcohol oxidation in acidic media. Methanol oxidation is a slow reaction that requires active multiple sites for the adsorption of methanol and the sites that can donate OH species for desorption of the adsorbed methanol residues [44]. Higher Pd atom content around Pt active sites decreases the probability of finding the neighboring Pt atoms for methanol chemisorption and hinders methanol oxidation. Accordingly, GDE4 (using the highest content of Pd around Pt), displaying poor activity in the methanol oxidation reaction, can be a good candidate for resolving the problem of methanol crossover in DMFCs.

3.3 Oxygen reduction reaction activity on GDEs in the presence of methanol

Figure 6A–D shows the ORR activity of the prepared GDEs in the presence of various methanol concentrations ranging from 0 M to 2 M CH_3OH. As it can be seen, all the GDEs show an increase in overpotential for the ORR in the presence of methanol (see Table 2). Under crossover conditions, the CH_3OH that reached the cathode must block the adsorption of oxygen on the cathode electrocatalysts, and thus will retard the electrochemical reduction of oxygen on the cathode. Catalytic oxidation of CH_3OH by the

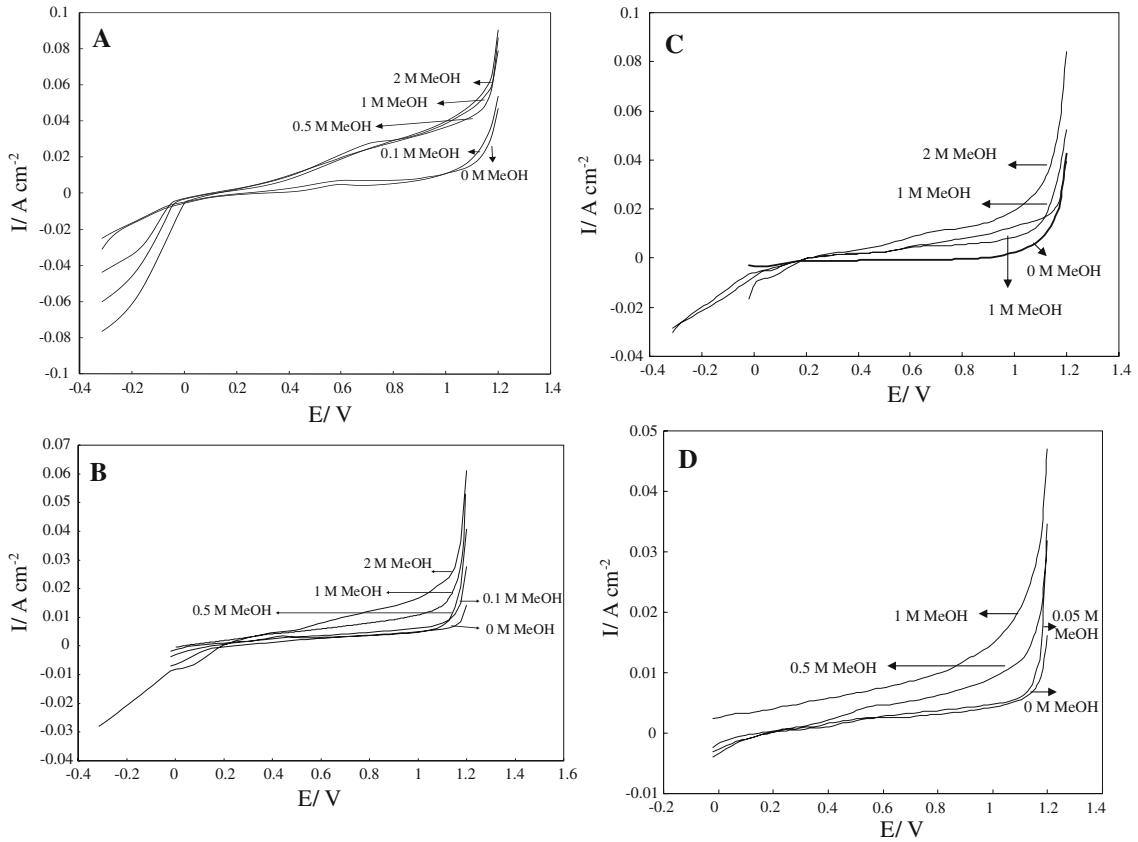

Fig. 6 Linear sweep voltammograms of ORR at room temperature in 2 M H_2SO_4 containing different amounts of methanol GDE1 (**A**), GDE2 (**B**), GDE3 (**C**), and GDE4 (**D**) and the scan rate of 5 mV s^{-1}

Table 2 Over potential of ORR in the absence and presence of methanol

Number of GDEs	Over potential of ORR (V) In H_2SO_4 (2 M)	Over potential of ORR (V) In H_2SO_4 (2 M) + MeOH (0.5 M)	Over potential of ORR (V) In H_2SO_4 (2 M) + MeOH (1 M)	Over potential of ORR (V) In H_2SO_4 (2 M) + MeOH (2 M)
GDE1	0.073	0.58	0.59	0.63
GDE2	0	0.049	0.10	0.26
GDE3	0.049	0.074	0.17	0.21
GDE4	0.024	0.049	0.073	0.24

oxygen adsorbed on the cathode may also decrease the steady-state concentration of the absorbed oxygen on the cathode. Products such as HCHO, CO, and CO_2 resulting from the catalytic oxidation of CH_3OH might also retard the electrochemical reduction of O_2 on the cathode. It is evident from Fig. 6 that methanol tolerance is higher for GDEs with Pt–Pd electrocatalysts. Higher methanol tolerance of GDEs with Pd-containing catalysts with respect to that of Pt alone can be more clearly seen in Fig. 7, where the potentials at 0.01 A cm^{-2} ($E_{0.01\,A\,cm^{-2}}$) from Fig. 6 (the choice of this value of current density in the region of oxygen reduction is arbitrary, being the trend similar for all values of the current density) are plotted against methanol concentration. The decrease of $E_{0.01\,A\,cm^{-2}}$ on GDE1 with the increase of methanol concentration is much higher compared with the other GDEs, showing that GDEs with Pt–Pd/CNT electrocatalysts (GDE2, GDE3, and GDE4) have higher resistance to the presence of methanol than GDE1. This result also shows that GDE4 has an optimum combination of Pt and Pd with the atomic ratio of 1:1 in its catalyst layer that acts as the best electrocatalyst for ORR in the presence of methanol. This result is in good agreement with our previous results in Sects. 3.1 and 3. 2.

It is shown in Fig. 7 that GDE4, which has a poor activity in MOR and a good activity in ORR (but not the best electrode in ORR), shows an excellent activity for

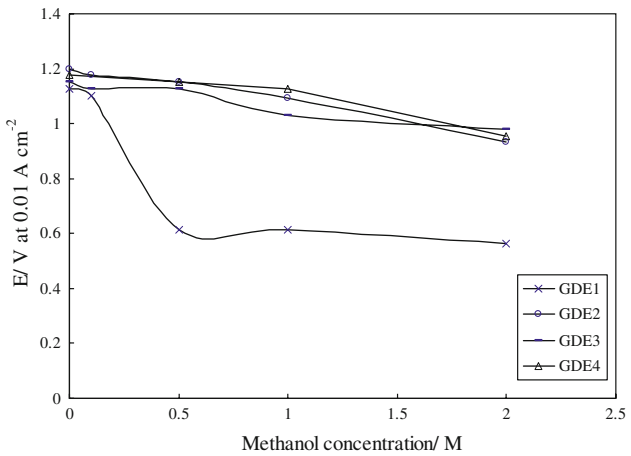

Fig. 7 Dependence of the potential at 0.01 A ($E_{0.01\ A}$) during the O_2 reduction in a 2 M H_2SO_4 solution on methanol concentration

ORR with higher methanol tolerance in the presence of methanol. As our previous results showed, GDE2 acts as the best electrode for ORR in the absence of methanol but its MOR activity is also higher than GDE3 and GDE4. On the other hand, Fig. 7 shows that oxygen reduction activity in the presence of methanol on GDE2 is easier than on GDE3 (see Table 2, the second column). This is because GDE2 has an excellent ORR activity in the absence of methanol. Behavior of GDE1, as the worse GDE for ORR in the presence of methanol, is in good agreement with our previous results.

3.4 Cyclic voltammetry

Figure 8A shows the cyclic voltammetric (CV) curves in 2 M H_2SO_4 solution without methanol. In the CVs obtained in a 2 M H_2SO_4 solution, the anodic peaks, appearing between −0.12 and 0.17 V, originate from desorption of atomic hydrogen on the electrocatalysts. Here, only single hydrogen desorption peak can be distinguished. The area of H-desorption after the deduction of the double layer region on the CV curves represents the charge passed for the H-desorption (Q_H) and is proportional to the electrochemical active area (EAA) of the electrocatalysts [45]. For GDE4, a very poorly resolved peak is observed in the hydrogen adsorption/desorption region.

It may be due to the blocking of the Pt active sites by Pd. In the preparation of the catalyst layer of GDE4, the smallest amount of Pt and the highest amount of Pd is used comparing to the other GDEs (Table 1). EAA for GDE1, GDE2, GDE3, and GDE4 is 111, 71, 59, and 27 $m^2\ g^{-1}$, respectively. Figure 8A also shows a single peak during the cathodic sweep. This peak is normally assigned to the oxide reduction profile of metals.

Figure 8B shows the cyclic voltammetric curves obtained for methanol oxidation in the oxygen saturated solutions of 2 M H_2SO_4 + 2 M CH_3OH. This figure also shows that the hydrogen adsorption/desorption profile almost disappears; this indicates that some sites are blocked by the presence of methanol.

The forward scan is attributable to methanol oxidation, forming Pt-adsorbed carbonaceous intermediates, including carbon monoxide (reaction 1), and CO_2 (reaction 2).

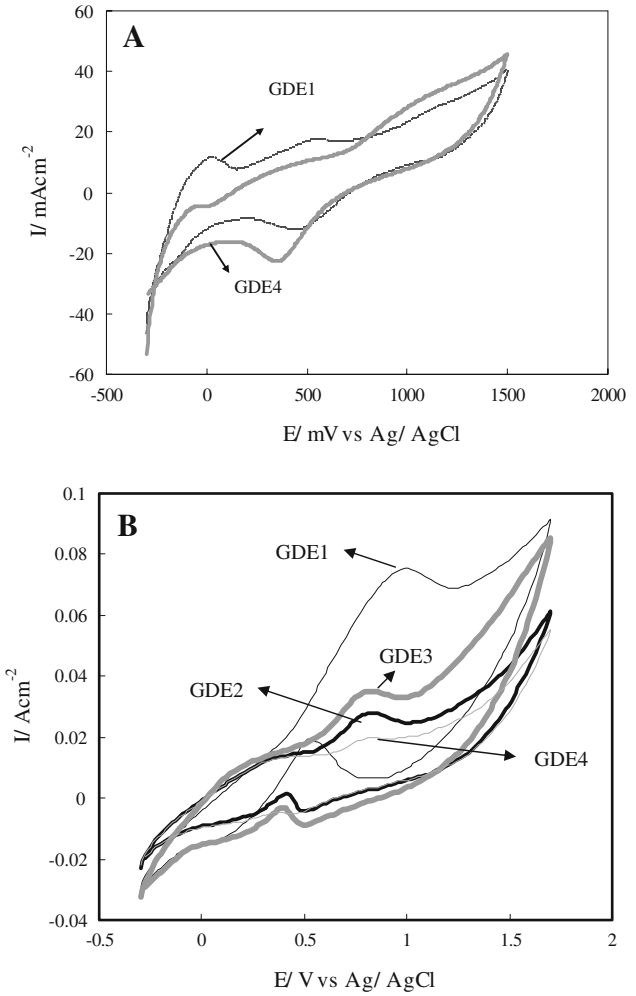

Fig. 8 Cyclic voltammograms of ORR on GDEs in 2 M H_2SO_4 (**A**), CVs of methanol oxidation on GDEs in 2 M H_2SO_4 + 2 M CH_3OH (**B**), and the scan rate of 50 mV s^{-1}

This adsorbed carbon monoxide (CO_{ads}) causes the loss of activity of the electrocatalyst [46–48]:

$$Pt + CH_3OH \rightarrow Pt - CO_{ads} + 4H^+ + 4e^-. \quad (1)$$

$$CH_3OH + H_2O \rightarrow CO_2 + 6H^+ + 6e^-. \quad (2)$$

The backward oxidation peak, shown in reaction 3, is attributed to the additional oxidation of the adsorbed carbonaceous species to carbon dioxide [48]:

$$Pt - CO_{ads} + H_2O \rightarrow Pt + CO_2 + 2H^+ + 2e^-. \quad (3)$$

Two strong peaks for the methanol oxidation in the positive and negative scan directions were observed at GDE1. However, the oxidation peaks of methanol at other GDEs (Fig. 8B, GDE4, GDE3, and GDE2) are much weaker than that at GDE1. Especially, the oxidation peaks of methanol at GDE4 almost disappear. It is illustrated that bimetallic electrocatalysts can significantly inhibit the oxidation of methanol at GDEs.

As shown in Fig. 8B, the onset potential on the electrode is 0.14, 0.26, 0.19, and 0.33 V (vs. Ag/AgCl) for the methanol oxidation on GDE1, GDE2, GDE3, and GDE4. The onset potential for the reaction on GDE1 is 50, 120, and 190 mV more negative than that on GDE3, GDE2, and GDE4, respectively, this indicates the enhanced electrode kinetics. The electrocatalytic activity, as measured by the peak current density in the forward scan, is 20 mA cm^{-2} for GDE4, 28 mA cm^{-2} for GDE2, 35 mA cm^{-2} for GDE3, and 75 mA cm^{-2} for GDE1. The results indicate that GDE1 possess the most suitable electrocatalytic properties for methanol electro-oxidation among the other GDEs.

In order to oxidize methanol and/or CO on a Pt surface via Langmuir–Hinselwood mechanism, adsorption of oxygen-containing species is needed. Therefore, by the experimental observations in Fig. 8B, it is clearly understood that the presence of Pd atoms in the catalysts inhibits the adsorption of oxygenated species on the anodic scan. It further suppresses the oxidation reaction of methanol.

3.5 Electrochemical impedance spectroscopy

In this study, the effect of methanol tolerance on ORR, on the Platinum and Platinum–Palladium alloys was studied by EIS in the GDE. The aqueous electrolyte-proton exchange membrane resistance related to the ohmic drop between the reference electrode and the electrode was subtracted. The impedance spectra (Fig. 9) showed two high frequency loops and one low frequency inductive loop. When the over potential value increases, the polarization resistance decreases, but the high frequency capacitive loops remain constant with the potential. This high frequency capacitive loop is either due to electronic contact problems between the electronic supply and the gas diffusion layer of GDE (RC parallel equivalent circuit), or to the ionic ohmic drop/double layer charging inside the catalyst layer [49].

The high frequency small loop is rather well-fitted by a contact resistance in parallel with a contact capacity in series with the electrode impedance. As a result, the total GDE impedance is the sum of the contact impedance and the usual electrode impedance.

On the other hand, the middle frequency capacitive loop decreases strongly, but the low inductive loop becomes proportionally more pronounced. These loops correspond to kinetics, adsorbed oxygenated intermediate species relaxation, and diffusion.

The composite capacitive loop at the intermediate frequencies is attributed to the charge transfer resistance plus double layer capacity and one of the relaxations of the two adsorbed intermediate species, while the low frequency inductive loop is explained by the second relaxation of the

adsorbed intermediate species. This inductive loop is specific to the presence of two electrochemical steps [50–52], and it is only slightly modified by the diffusion effect.

Most of the studies in the literature [53–56] did not show any low frequency inductive loop, and only two papers [57, 58] showed inductive points or an inductive loop. In fact, these studies generally involved a thick active layer or a thick gas diffusion layer. The associated diffusion is a thin film like type diffusion.

The EIS is a power tool for elucidating the mechanism of a reaction involving multi-step kinetics, since it offers the advantage of separating different rate processes in the frequency domain, and, therefore, provides a better insight on the reaction mechanism of the electrode system. One prerequisite for an accurately quantitative EIS measurement is that the fluctuation of the electrode potential must be much lower than the small perturbation potential signal. Figure 10 shows the Nyquist impedance spectra of GDE4 for 2 M H_2SO_4 electrolyte. These impedance behaviors were almost under the control of pure kinetics because the mass-transfer limitation of oxygen was significantly minimized using O_2 saturated electrolyte. The results showed the same regions reported in Fig. 9. It is noteworthy that the low frequency inductive loop was probably due to the relaxation of the adsorbed intermediates for ORR that was seldom observed in the previous EIS studies (such as Fig. 9). This loop was often masked by the oxygen diffusion limitation in the bulk solutions or by the anode influence in the complete fuel cell investigations, the inductive loop was critical to the analysis of the reaction kinetics. Figure 11 shows the Nyquist impedance spectra of GDE4 when 0.5 M methanol was added to the H_2SO_4 electrolyte. These impedance spectra, along with those in Fig. 10, are all in a good shape, and indicate that the process of EIS measurements by these systems was very stable.

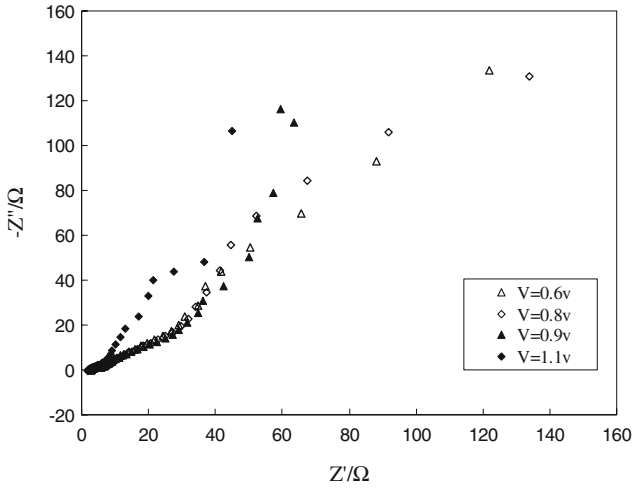

Fig. 9 Nyquist plots for ORR on GDE1 in 2 M H_2SO_4 subjected to various applied potentials of 600, 800, 900, and 1,100 mV

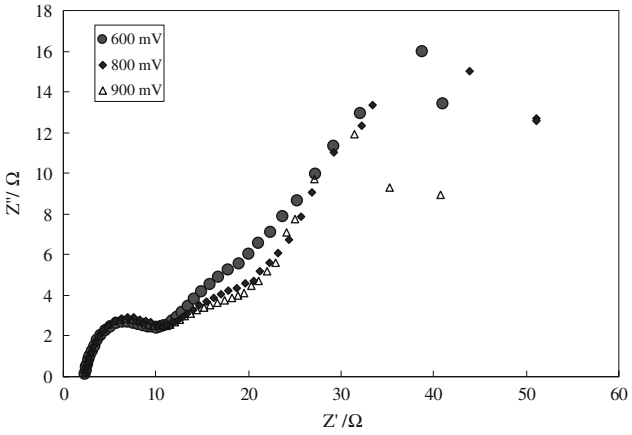

Fig. 10 Nyquist plots for ORR on GDE4 in 2 M H_2SO_4 subjected to various applied potentials 600, 800, and 900 mV

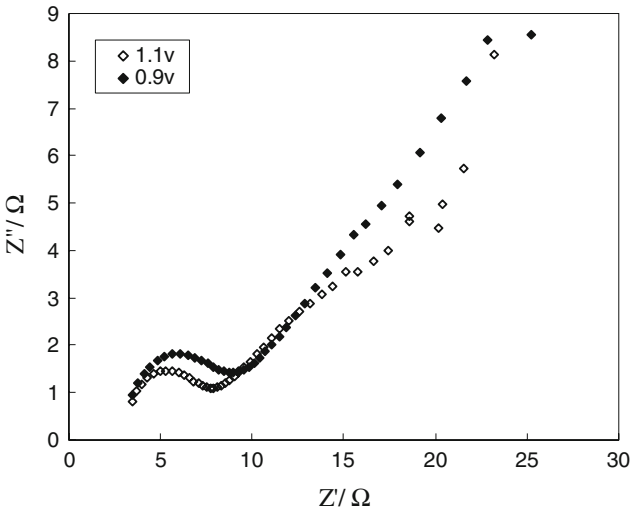

Fig. 11 Nyquist plots for ORR on GDE4 in 2 M H_2SO_4 + 0.5 M CH_3OH subjected to various applied potentials 900 and 1,100 mV

Similar to Figs. 9 and 10, a high frequency loop at high frequencies, a capacitive loop at medium frequency and a low frequency inductive loop at low frequencies are also observed in Fig. 11, which indicate the ORR mechanism.

4 Conclusion

The oxygen reduction reaction in the absence and presence of methanol on bimetallic Pt–Pd/CNT catalysts and their application to resolve the problem of methanol crossover in a direct methanol fuel cell were studied.

Clearly, a compromise between the performance of both ORR and MOR reactions is necessary to develop improved cathodic catalysts for DMFC.

The reaction kinetics showed that GDE1, which acted as an excellent electrode for MOR, acted as a worse electrode for ORR in the absence and in the presence of methanol. The results also showed that with increasing Pd content in the electrocatalyst of GDEs, methanol oxidation becomes harder. GDE4 (with highest content of Pd) that is less active for MOR, acted as the best one for ORR in the presence of methanol.

The four GDEs' ability to maintain their oxygen reduction activity in the presence of methanol ranked as GDE4 > GDE2 > GDE3 > GDE1.

This may be explained as follows: it is well-known that at least three adjacent Pt sites are necessary for methanol oxidation to activate the chemisorption of methanol. The probability of obtaining three adjacent Pt sites on the Pt–Pd/CNT catalyst is lower, since Pt nanoparticles are separated by Pd atoms. On the other hand, the addition of palladium will partly block the contact between Pt nanoparticles and methanol molecules, which in turn will suppress methanol oxidation on the Pt–Pd/CNT catalyst. Therefore, the high methanol tolerance could be ascribed to the unique surface structure of the Pt–Pd/CNT catalyst with the atomic ratio of 1:1 catalyst that suppresses methanol oxidation.

The results obtained by electrochemical techniques indicated a promoting effect of the bimetallic catalyst in enhancing the ORR and a better tolerance to methanol, and that Pt–Pd especially with the atomic ratio of 1:1 (used to prepare GDE4) can be an economical candidate to replace Pt as a cathodic fuel cell catalyst, especially for DMFCs.

References

1. Golabi SM, Golikand AN (2002) J Electroanal Chem 521:161
2. Hogarth M, Christensen P, Hamnett A et al (1997) J Power Sources 69:113
3. Jarvi TD, Stuve S, Sriramulu EM (1997) J Phys Chem B 101:3646
4. Lee K, Savadogo O, Ishihara A et al (2006) J Electrochem Soc 153:A20
5. Yang H, Alonso-Vante N, Léger JM et al (2004) J Phys Chem B 108:1938
6. Song S, Wang Y, Tsiakaras P et al (2008) Appl Catal B 78:381
7. McGovern M, Waszczuk P, Wieckowski A (2006) Electrochim Acta 51:1194–1198
8. Behm RJ, Jusys Z (2006) J Power Sources 154:327–342
9. Wang JT, Wasmus S, Savinell R (1996) J Electrochem Soc 143:1233–1239
10. Lamy C, Lima A, LeRhun V et al (2002) J Power Sources 105:283
11. Bron M, Bogdanoff P, Fiechter S et al (2001) J Electroanal Chem 500:510
12. Schmidt TJ, Paulus UA, Gasteiger HA et al (2000) J Electrochem Soc 147:2620
13. Jiang R, Chu D (2000) J Electrochem Soc 147:4605
14. Convert P, Coutanceau C, Crouigneau P et al (2001) J Appl Electrochem 31:945
15. Yang H, Alonso-Vante N, Lamy C et al (2005) Electrochem Soc 152:A704
16. Golikand AN, Shahrokhian S, Asgari M et al (2005) J Power Sources 144:21
17. Lee SA, Park KW, Choi JH et al (2002) J Electrochem Soc 106:1869
18. Antolini E, Salgado JRC, Gonzalez ER (2006) J Power Sources 155:161
19. Antolini E, Salgado JRC, Gonzalez ER (2006) Appl Catal B 63:137
20. Scott K, Yuan W, Cheng H (2007) J Appl Electrochem 37:21
21. Fortunelli A, Velasco AM (2002) J Mol Theochem 586:17
22. Xia D, Chen G, Wang Z et al (2006) Chem Mater 18:5746
23. Stassi A, D'Urso C, Baglio V et al (2006) J Appl Electrochem 36:1143
24. Koffi RC, Coutanceau C, Garnier E et al (2005) Electrochim Acta 50:4117
25. Markovic NM, Ross PN (2002) Surf Sci Rep 45:121
26. Lamy C, Lima A, Rhun VL et al (2002) J Power Sources 105:283
27. Gasteiger HA, Markovic NM, Ross PN et al (1994) Electrochim Acta 39:1825
28. Antolini E, Salgado JRC, Santos AM et al (2005) Electrochem Solid State Lett 8:A226
29. Antolini E, Salgado JRC, Gonzalez ER (2006) J Power Sources 155:161
30. Stassi A, D'Urso C, Baglio V et al (2006) J Appl Electrochem 36:1143
31. Markovic NM, Gasteiger HA, Ross PN et al (1995) Electrochim Acta 40:91
32. Goikovic SL, Vidakovic TR, Durovic DR (2003) Electrochim Acta 48:3607
33. Christensen PA, Hamnett A, Troughton GL (1993) J Electroanal Chem 362:207
34. Park K, Han D, Sung Y (2006) J Power Sources 163:82
35. Mukerjee S, Srinivasan S, Soriaga MP et al (1995) J Electrochem Soc 142:1409
36. Maynard HL, Meyers JP (2002) J Vac Sci Technol B 20:1287
37. Shao MH, Huang T, Liu P et al (2006) Langmuir 22:10409–10415
38. Nozad Golikand A, Lohrasbi E, Ghannadi Maragheh M et al (2008) J Appl Electrochem 38:869
39. Mukerjee S, Srinivasan S, Soriaga MP (1995) J Phys Chem 99:4577
40. Gebel G, Aldebert P, Pineri M (1987) Macromolecules 20:1425
41. Norskov JK, Rossmeisl J, Logadottir A et al (2004) J Phys Chem B 108:17886
42. Gasteiger HA, Kocha SS, Sompalli B et al (2005) Appl Catal B 46:9
43. Mukerjee S, Srinivasan S, Soriaga MP et al (1995) J Electrochem Soc 142:1409
44. Bagotzsky VS, Vassiliev YB, Khazova OA (1977) J Electroanal Chem 81:229
45. Lee SJ, Mukerjee S, McBreen J et al (1998) Electrochim Acta 43:3693
46. Liu Z, Ling XY, Su X et al (2004) J Phys Chem B 108:8234
47. Huang J, Liu Z, He C, Gan LM (2005) J Phys Chem B 109:16644
48. Hoogers G (2003) Fuel cell technology handbook. CRC Press, Boca Raton, FL
49. Eikerling M, Kornysher AA (1999) J Electroanal Chem 475:107
50. Kadiri F E, Durand R, Faure R (1990) 41st ISE meeting, Paraque
51. Kadiri FEl, Durand R, Belacadi S (1990). In: C. Gabrielli (eds) Proceeding of the Fourth Forum on Electrochemical Impedance, Paris, 161

52. Diard JP, Le Gorrec B, Montella C et al (1993) J Electroanal Chem 352:27
53. Springer TE, Raistrick ID (1987) ECS symposium 12:152
54. Springer TE, Raistrick ID (1989) J Electrochem Soc 136:1594
55. Raistrick ID (1990) Electrochim Acta 35:1579
56. Dasilva SL, Ticianelli EA (1995) J Electroanal Chem 391:101
57. Arico A, Alderucci V, Antonucci V et al (1992) Electrochim Acta 37:523
58. Pyun SI, Ryu YG (1996) J Power sources 62:1